Electromagnetic radiation and scattering for a gap in a corner backed by a cavity filled with DNG metamaterial

Oguzhan Akgol,[1] Danilo Erricolo,[1] and Piergiorgio L. E. Uslenghi[1]

Received 7 July 2010; revised 16 March 2011; accepted 4 May 2011; published 4 August 2011.

[1] A partially covered cavity, or trench, located along the edge of two intersecting metallic walls perpendicular to each other is considered. The cross section of the cavity is a quarter ellipse and is slotted along the interfocal distance. The cavity is filled with a double-negative (DNG) metamaterial that is isoimpedance to the material filling the half-space above the trench. This two-dimensional boundary value problem is solved exactly, in the frequency domain, when the primary field is either a plane wave of arbitrary polarization and direction of incidence or an electric or magnetic line source. Numerical results are exhibited and discussed.

Citation: Akgol, O., D. Erricolo, and P. L. E. Uslenghi (2011), Electromagnetic radiation and scattering for a gap in a corner backed by a cavity filled with DNG metamaterial, *Radio Sci.*, *46*, RS4005, doi:10.1029/2010RS004471.

1. Introduction

[2] We consider the two-dimensional geometry of Figure 1 where a partially covered cavity is located at the corner of two metallic walls perpendicular to each other. The cavity has a cross section that is a quarter ellipse, and is slotted from the focus to the center of the ellipse. The cavity is partially covered by a thin metallic strip that extends from the focal line away from the central line of the ellipse, as part of the metallic wall under which the cavity is flush mounted. The cavity is filled with a double-negative lossless metamaterial whose electric permittivity and magnetic permeability are real and opposite to the corresponding parameters of the quarter-space above the cavity. Causality requires that the index of refraction of the DNG material be negative and its intrinsic impedance positive.

[3] Two types of sources are considered. One is a plane wave with arbitrary direction of incidence in the quarter space ($x > 0$, $y > 0$) and polarized with the electric or the magnetic field parallel to the z axis. The other one is an electric or magnetic line source parallel to the z axis. This two-dimensional boundary value problem is solved exactly, in the frequency domain. In elliptic cylindrical coordinates, the primary and secondary field components are expanded in infinite series of eigenfunctions that are products of radial and angular Mathieu functions, where the Stratton-Chu normalization is adopted [see, e.g., *Stratton*, 1941; *Staff of the Computation Laboratory*, 1967; *Bowman et al.*, 1987]. Since the angular Mathieu functions are the same for positive and negative refractive index, it is possible to determine analytically the modal expansion coefficients of the secondary fields, by imposing the boundary conditions.

[4] The only two-dimensional problem involving radiation and scattering by a cavity flush mounted under a metallic plane for which an exact analytical solution exists is that of a slotted semielliptical channel [*Uslenghi*, 1992, 2004a]. A related geometry is the cavity-backed gap in a corner [*Uslenghi*, 1999; *Erricolo and Uslenghi*, 2005]. These geometries involve materials inside and outside the channel that are isorefractive to each other. Recently, the analysis performed by *Uslenghi* [1992, 2004a] was extended to the case of a trench filled with DNG metamaterial [*Akgol et al.*, 2009a, 2009b]. The present work is an extension of the geometry analyzed by *Uslenghi* [1999] and *Erricolo and Uslenghi* [2005] to the case of a corner cavity filled with DNG metamaterial.

[5] Numerical results are shown for fields both inside and outside the cavity, for several cavity configurations and different primary sources.

2. Geometry of the Problem

[6] A cross-sectional view of the structure in a plane z = constant is shown in Figure 1. It is identical to that considered by *Erricolo and Uslenghi* [2005], except for the material filling the trench.

[7] The metallic walls $OA(x = 0)$ and $OE(y = 0)$ are perpendicular to each other. The trench OBC is flush mounted under the horizontal wall OE, and its cross section is a quarter ellipse with semimajor axis OC and semiminor axis OB. The wall OE is slotted along the slit of width OD equal to half the interfocal distance d of the elliptical trench. The trench is partially covered by the thin metal baffle DC.

[8] The rectangular coordinates (x, y, z) are related to the elliptic cylinder coordinates (u, v, z) by

$$x = \frac{d}{2}\cosh u \cos v,$$
$$y = \frac{d}{2}\sinh u \sin v, \qquad (1)$$
$$z = z,$$

[1]Department of Electrical and Computer Engineering, University of Illinois at Chicago, Chicago, Illinois, USA.

0048-6604/11/2010RS004471

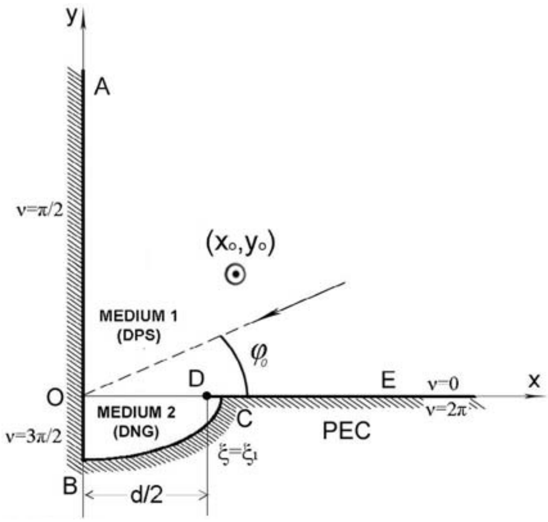

Figure 1. Geometry of the problem.

where $0 \le u < \infty$, $0 \le v \le 2\pi$, $-\infty < z < \infty$. Sometimes, it is expedient to introduce the coordinates

$$\xi = \cosh u, \quad \eta = \cos v, \tag{2}$$

with $1 \le \xi < \infty$ and $-1 \le \eta \le 1$. However, the advantage of using (u, v) instead of (ξ, η) is the removal of sign ambiguities since the pair (u, v) corresponds to only one pair (ξ, η) but the reverse is not true. Curves with u (ξ) constant are ellipses and curves with v (η) constant are hyperbolas. The variable ξ asymptotically approaches $2r/d$, where r is the distance from the origin. The variable v represents the angle between the asymptote $y = x \tan v$ and the hyperbola whose parametric equations are (1) when v is held constant. Additional information on the elliptic cylinder coordinate system may be found in the work by *Stratton* [1941].

[9] Outside the cavity, the electric permittivity is ε and the magnetic permeability is μ, whereas inside the cavity the same quantities become $-\varepsilon$ and $-\mu$, respectively. Therefore, the intrinsic impedance is the same inside and outside the cavity. More generally, this type of analysis could be performed under the less restrictive condition that the intrinsic impedances inside and outside the trench be different from each other. However, the formulas would become more complicated because of the introduction of an additional parameter.

[10] The wave vector is $k = \sqrt{\varepsilon\mu}$ outside the cavity and $-\sqrt{\varepsilon\mu}$ inside the cavity. We define a dimensionless parameter $c = kd/2$ in the material outside the cavity and $-c$ inside the cavity filled with DNG material. Causality, and not just the radiation condition, dictates that in a DNG metamaterial the signs of the square roots must be chosen so that the refractive index is negative but the intrinsic impedance is positive [see *Ziolkowski and Heyman*, 2001].

3. Plane Wave Incidence

3.1. E Polarization

[11] Consider a plane wave incident perpendicularly to the trench axis and polarized parallel to z axis, with primary electric field

$$\boldsymbol{E}^i = \hat{z}E^i_{1z} = \hat{z}\exp[jk(x\cos\varphi_0 + y\sin\varphi_0)]. \tag{3}$$

The incident field may be expanded in a series of elliptic-cylinder functions [*Bowman et al.*, 1987]

$$E^i_{1z} = \sqrt{8\pi}\sum_{m=0}^{\infty} j^m \times \left[\frac{1}{N_m^{(e)}}\mathrm{Re}_m^{(1)}(c,u)\mathrm{Se}_m(c,v)\mathrm{Se}_m(c,\varphi_0) + \frac{1}{N_m^{(o)}}\mathrm{Ro}_m^{(1)}(c,u)\mathrm{So}_m(c,v)\mathrm{So}_m(c,\varphi_0)\right]. \tag{4}$$

The total electric field in medium 1 can be written as the sum of a geometric-optics field E^{go}_{1z} due to the corner reflector without the trench and a diffracted field E^d_{1z} due to the presence of the trench

$$E_{1z} = E^{go}_{1z} + E^d_{1z}. \tag{5}$$

The geometric-optics field is the sum of four terms

$$E^{go}_{1z} = E^i_{1z} + E^{OE}_{1z} + E^{OA}_{1z} + E^{OA,OE}_{1z}, \tag{6}$$

where, referring to Figure 2, the field E^{OE}_{1z} corresponds to a wave with incidence angle $2\pi - \varphi_0$, with respect to the negative x axis, multiplied by a reflection coefficient -1, the field E^{OA}_{1z} corresponds to a wave with incidence angle $\pi - \varphi_0$ multiplied by a reflection coefficient -1, and the field $E^{OA,OE}_{1z}$ corresponds to a doubly reflected wave, i.e., a wave with incidence angle $\pi + \varphi_0$ and reflection coefficient 1.

[12] When the even and odd functions of φ_0 are separated out in the various field components, it is found that the overall geometric-optics field is

$$E^{go}_{1z} = 8\sqrt{2\pi}\sum_{l=1}^{\infty}\frac{(-1)^l}{N_{2l}^{(o)}}\mathrm{Ro}_{2l}^{(1)}(c,u)\mathrm{So}_{2l}(c,v)\mathrm{So}_{2l}(c,\varphi_0). \tag{7}$$

The diffracted field can be written as

$$E^d_{1z} = 8\sqrt{2\pi}\sum_{l=1}^{\infty}\frac{(-1)^l}{N_{2l}^{(o)}}a_l\mathrm{Ro}_{2l}^{(4)}(c,u) \times \mathrm{So}_{2l}(c,v)\mathrm{So}_{2l}(c,\varphi_0). \tag{8}$$

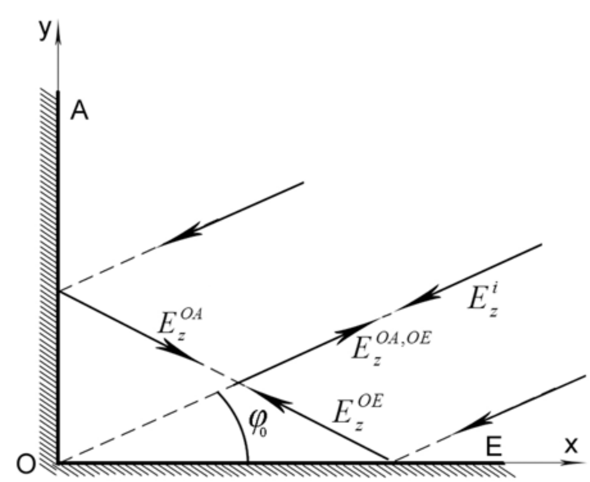

Figure 2. Geometric-optics contribution for plane wave incidence.

The total electric field inside the trench is

$$E_{2z} = 8\sqrt{2\pi}\sum_{l=1}^{\infty}\frac{(-1)^l}{N_{2l}^{(o)}}b_l \times \left[\frac{\mathrm{Ro}_{2l}^{(4)}(-c,u_1)}{\mathrm{Ro}_{2l}^{(1)}(-c,u_1)}\mathrm{Ro}_{2l}^{(1)}(-c,u) - \mathrm{Ro}_{2l}^{(4)}(-c,u)\right] \times \mathrm{So}_{2l}(c,v)\mathrm{So}_{2l}(c,\varphi_0). \quad (9)$$

The magnetic field is obtained using the relation

$$\boldsymbol{H}_{1,2} = \frac{j}{\pm cZ\sqrt{\xi^2-\eta^2}}\left(\frac{\partial E_{(1,2)z}}{\partial v}\hat{u} - \frac{\partial E_{(1,2)z}}{\partial u}\hat{v}\right). \quad (10)$$

[13] The modal coefficients can be found by applying the boundary conditions. The tangential component of the total electric and magnetic fields in both media are equal across $u = 0$,

$$E_{1z}|_{u=0} = E_{2z}|_{u=0},\ H_{1v}|_{u=0} = -H_{2v}|_{u=0}. \quad (11)$$

[14] Mode matching is possible because the Mathieu angular functions inside the DNG material have a parameter $-c < 0$ and are related to the Mathieu functions for $c > 0$ by

$$\mathrm{Se}_m(-c,v) = \mathrm{Se}_m(c,v) \quad (12)$$

$$\mathrm{So}_m(-c,v) = \mathrm{So}_m(c,v), \quad (13)$$

since the expansion coefficients depend on $(\pm c)^2$. The Mathieu radial functions have the same expansion coefficients as the Mathieu angular functions, but the arguments of the various Bessel functions in the series expansions contain the quantity $c\exp(\pm u)$ so that the Mathieu radial functions for $-c < 0$ have different values from the Mathieu radial functions for $c > 0$. Therefore, applying the boundary conditions yields the modal coefficients a_l and b_l as

$$a_l = -\frac{\mathrm{Ro}_{2l}^{(4)}(-c,0)\mathrm{Ro}_{2l}^{(1)\prime}(c,0)}{\Delta_1}, \quad (14)$$

$$b_l = -\frac{\mathrm{Ro}_{2l}^{(1)\prime}(c,0)\mathrm{Ro}_{2l}^{(4)}(c,0)}{\Delta_1}, \quad (15)$$

where

$$\Delta_1 = \mathrm{Ro}_{2l}^{(4)}(-c,0)\mathrm{Ro}_{2l}^{(1)\prime}(-c,0)\frac{\mathrm{Ro}_{2l}^{(4)}(-c,u_1)}{\mathrm{Ro}_{2l}^{(1)}(-c,u_1)} + \mathrm{Ro}_{2l}^{(4)\prime}(c,0)\mathrm{Ro}_{2l}^{(4)}(-c,0) - \mathrm{Ro}_{2l}^{(4)}(c,0)\mathrm{Ro}_{2l}^{(4)\prime}(-c,0). \quad (16)$$

[15] Within the quarter space ($x > 0$, $y > 0$), the bistatic RCS $\sigma^{(e)}(\phi)$ is, in general, given by [see, e.g., *Bowman et al.*, 1987]

$$\sigma^{(e)}(\phi) = \lim_{\rho\to\infty} 2\pi\rho\frac{|\mathbf{E}^{\mathbf{s}}|}{|\mathbf{E}^{\mathbf{i}}|} \quad (17)$$

and in the case of this partially covered trench it becomes

$$\frac{\sigma^{(e)}(\phi)}{\lambda} = 128\pi\left|\sum_{l=1}^{\infty}\frac{a_l}{N_{2l}^{(o)}}\mathrm{So}_{2l}(c,v)\mathrm{So}_{2l}(c,\varphi_0)\right|^2, \quad (18)$$

which is obtained by evaluating $\mathrm{Ro}_{2l}^{(4)}(c, u)$ in (8) with an asymptotic expression of the Mathieu radial function [*Uslenghi*, 2004b].

3.2. H Polarization

[16] The analysis is similar to that for E polarization, hence only the results are given. The incident magnetic field is

$$\boldsymbol{H}^i = \hat{z}H_{1z}^i, \quad (19)$$

$$H_{1z}^i = \exp[jk(x\cos\varphi_0 + y\sin\varphi_0)] = \sqrt{8\pi}\sum_{m=0}^{\infty}\left[\frac{j^m}{N_m^{(e)}}\mathrm{Re}_m^{(1)}(c,u)\mathrm{Se}_m(c,v)\mathrm{Se}_m(c,\varphi_0) + \frac{j^m}{N_m^{(o)}}\mathrm{Ro}_m^{(1)}(c,u)\mathrm{So}_m(c,v)\mathrm{So}_m(c,\varphi_0)\right]. \quad (20)$$

[17] The total magnetic field in medium 1 is

$$H_{1z} = H_{1z}^{go} + H_{1z}^{d}, \quad (21)$$

where the geometric-optics field H_{1z}^{go} is

$$H_{1z}^{go} = 8\sqrt{2\pi}\sum_{l=0}^{\infty}\frac{(-1)^l}{N_{2l}^{(e)}}\mathrm{Re}_{2l}^{(1)}(c,u)\mathrm{Se}_{2l}(c,v)\mathrm{Se}_{2l}(c,\varphi_0), \quad (22)$$

corresponding to the sum of four plane waves that are equivalent to those of Figure 2, provided that the electric field is replaced with a z directed magnetic field and all reflection coefficients are 1. Only the even Mathieu functions of even order appear because of the boundary conditions of the two metallic walls. The diffracted field due to the slotted trench is

$$H_{1z}^{d} = 8\sqrt{2\pi}\sum_{l=0}^{\infty}\frac{(-1)^l}{N_{2l}^{(e)}}c_l\mathrm{Re}_{2l}^{(4)}(c,u) \times \mathrm{Se}_{2l}(c,v)\mathrm{Se}_{2l}(c,\varphi_0), \quad (23)$$

the field inside the trench is

$$H_{2z} = 8\sqrt{2\pi}\sum_{l=0}^{\infty}\frac{(-1)^l}{N_{2l}^{(e)}}d_l \times \left[\frac{\mathrm{Re}_{2l}^{(4)\prime}(-c,u_1)}{\mathrm{Re}_{2l}^{(1)\prime}(-c,u_1)}\mathrm{Re}_{2l}^{(1)}(-c,u) - \mathrm{Re}_{2l}^{(4)}(-c,u)\right] \times \mathrm{Se}_{2l}(c,v)\mathrm{Se}_{2l}(c,\varphi_0), \quad (24)$$

where the prime means the derivative with respect to u. The electric field is obtained from

$$\boldsymbol{E}_{1,2} = \frac{jZ}{\pm c\sqrt{\xi^2-\eta^2}}\left(-\frac{\partial H_{(1,2)z}}{\partial v}\hat{u} + \frac{\partial H_{(1,2)z}}{\partial u}\hat{v}\right). \quad (25)$$

[18] The boundary conditions are

$$H_{1z}|_{u=0} = H_{2z}|_{u=0},\ E_{1v}|_{u=0} = -E_{2v}|_{u=0}, \quad (26)$$

which yield the expansion coefficients

$$c_l = -\frac{\mathrm{Re}_{2l}^{(4)\prime}(-c,0)\mathrm{Re}_{2l}^{(1)}(c,0)}{\Delta_2}, \tag{27}$$

$$d_l = \frac{\mathrm{Re}_{2l}^{(4)\prime}(c,0)\mathrm{Re}_{2l}^{(1)}(c,0)}{\Delta_2}, \tag{28}$$

where

$$\Delta_2 = \mathrm{Re}_{2l}^{(4)}(c,0)\mathrm{Re}_{2l}^{(4)\prime}(-c,0) + \mathrm{Re}_{2l}^{(4)\prime}(c,0) \cdot \left[\frac{\mathrm{Re}_{2l}^{(4)\prime}(-c,u_1)}{\mathrm{Re}_{2l}^{(1)\prime}(-c,u_1)}\mathrm{Re}_{2l}^{(1)}(-c,0) - \mathrm{Re}_{2l}^{(4)}(-c,0)\right]. \tag{29}$$

[19] The bistatic RCS $\sigma^{(h)}(\phi)$ of the partially covered trench is

$$\frac{\sigma^{(h)}(\phi)}{\lambda} = 128\pi\left|\sum_{l=1}^{\infty}\frac{c_l}{N_{2l}^{(e)}}\mathrm{Se}_{2l}(c,v)\mathrm{Se}_{2l}(c,\varphi_0)\right|^2. \tag{30}$$

4. Line Source Incidence

4.1. E Polarization

[20] Consider an electric line source parallel to the z axis and located at $(x_0, y_0) \equiv (u_0, v_0)$ whose primary electric field is

$$\boldsymbol{E}^i = \hat{z}E_z^i = \hat{z}H_0^{(2)}(kR), \tag{31}$$

where

$$R = \sqrt{(x-x_0)^2 + (y-y_0)^2} \tag{32}$$

is the distance between the line source and the observation point $(x, y) \equiv (u, v)$. The incident field may be expanded in a series of elliptic-cylinder functions [*Bowman et al.*, 1987]

$$\begin{aligned} E_{1z}^i &= H_0^{(2)}(kR) \\ &= 4\sum_{m=0}^{\infty}\left[\frac{1}{N_m^{(e)}}\mathrm{Re}_m^{(1)}(c,u_<)\mathrm{Re}_m^{(4)}(c,u_>)\mathrm{Se}_m(c,v)\times\mathrm{Se}_m(c,v_0)\right. \\ &\quad \left. + \frac{1}{N_m^{(o)}}\mathrm{Ro}_m^{(1)}(c,u_<)\mathrm{Ro}_m^{(4)}(c,u_>)\times\mathrm{So}_m(c,v)\mathrm{So}_m(c,v_0)\right], \end{aligned} \tag{33}$$

where $u_<$ ($u_>$) is the smaller (larger) between u and u_0.

[21] In the quarter space ($x \geq 0$, $y \geq 0$) outside the trench, the total electric field E_{1z} may be written as the sum of the diffracted field and the geometrical-optics field. The geometrical-optics field E_{1z}^{go} is the total field that would be present in the absence of the trench and is the sum of the fields due to four line sources, i.e., the primary line source and its three images

$$E_{1z}^{go} = H_0^{(2)}(kR) - H_0^{(2)}(kR_1) - H_0^{(2)}(kR_2) + H_0^{(2)}(kR_3), \tag{34}$$

where

$$R_1 = \sqrt{(x-x_0)^2 + (y+y_0)^2}, \tag{35}$$

$$R_2 = \sqrt{(x+x_0)^2 + (y-y_0)^2}, \tag{36}$$

$$R_3 = \sqrt{(x+x_0)^2 + (y+y_0)^2}. \tag{37}$$

[22] Referring to Figure 3, the image line S_1 is located at $(x_0, -y_0) \equiv (u_0, 2\pi - v_0)$, the image line S_2 at $(-x_0, y_0) \equiv (u_0, \pi - v_0)$, and the image line S_3 at $(-x_0, -y_0) \equiv (u_0, \pi + v_0)$.

[23] By expanding the Hankel functions in series of elliptic-cylinder functions and utilizing properties of the angular Mathieu functions, it can be found that

$$E_{1z}^{go} = 16\sum_{l=0}^{\infty}\frac{1}{N_{2l}^{(o)}}\mathrm{Ro}_{2l}^{(1)}(c,u_<)\mathrm{Ro}_{2l}^{(4)}(c,u_>)\times\mathrm{So}_{2l}(c,v)\mathrm{So}_{2l}(c,v_0), \tag{38}$$

which involves only odd Mathieu functions of even order. The diffracted field E_{1z}^d due to the presence of the trench in ($x \geq 0$, $y \geq 0$) and the total field inside the trench are given by, on consideration of the boundary conditions,

$$E_{1z}^d = 16\sum_{l=1}^{\infty}\frac{e_l}{N_{2l}^{(o)}}\mathrm{Ro}_{2l}^{(4)}(c,u_0)\mathrm{Ro}_{2l}^{(4)}(c,u)\times\mathrm{So}_{2l}(c,v)\mathrm{So}_{2l}(c,v_0) \tag{39}$$

$$\begin{aligned} E_{2z} &= 16\sum_{l=1}^{\infty}\frac{f_l}{N_{2l}^{(o)}}\mathrm{Ro}_{2l}^{(4)}(-c,u_0) \\ &\quad\times\left[\frac{\mathrm{Ro}_{2l}^{(4)}(-c,u_1)}{\mathrm{Ro}_{2l}^{(1)}(-c,u_1)}\mathrm{Ro}_{2l}^{(1)}(-c,u) - \mathrm{Ro}_{2l}^{(4)}(-c,u)\right] \\ &\quad\times\mathrm{So}_{2l}(-c,v)\mathrm{So}_{2l}(-c,v_0). \end{aligned} \tag{40}$$

[24] The magnetic field is still related to the electric field by (10). The unknown modal coefficients e_l and f_l are determined by imposing the continuity of the total tangential electric and magnetic fields across the interface $\xi = 1$ or $u = 0$, yielding

$$e_l = -\mathrm{Ro}_{2l}^{(4)}(-c,u_0)\mathrm{Ro}_{2l}^{(4)}(-c,0)\mathrm{Ro}_{2l}^{(1)\prime}(c,0)\times\frac{\mathrm{Ro}_{2l}^{(4)}(c,u_0)}{\Delta_3}, \tag{41}$$

$$f_l = -\frac{\mathrm{Ro}_{2l}^{(1)\prime}(c,0)\mathrm{Ro}_{2l}^{(4)}(c,u_0)\mathrm{Ro}_{2l}^{(4)}(c,0)\mathrm{Ro}_{2l}^{(4)}(c,u_0)}{\Delta_3}, \tag{42}$$

where

$$\begin{aligned} \Delta_3 &= \mathrm{Ro}_{2l}^{(4)}(c,u_0)\mathrm{Ro}_{2l}^{(4)}(-c,u_0)\Big[\mathrm{Ro}_{2l}^{(4)}(c,0) \\ &\quad\times\left(\frac{\mathrm{Ro}_{2l}^{(4)}(-c,u_1)}{\mathrm{Ro}_{2l}^{(1)}(-c,u_1)}\mathrm{Ro}_{2l}^{(1)\prime}(-c,0) - \mathrm{Ro}_{2l}^{(4)\prime}(-c,0)\right) \\ &\quad + \mathrm{Ro}_{2l}^{(4)}(-c,0)\mathrm{Ro}_{2l}^{(4)\prime}(c,0)\Big]. \end{aligned} \tag{43}$$

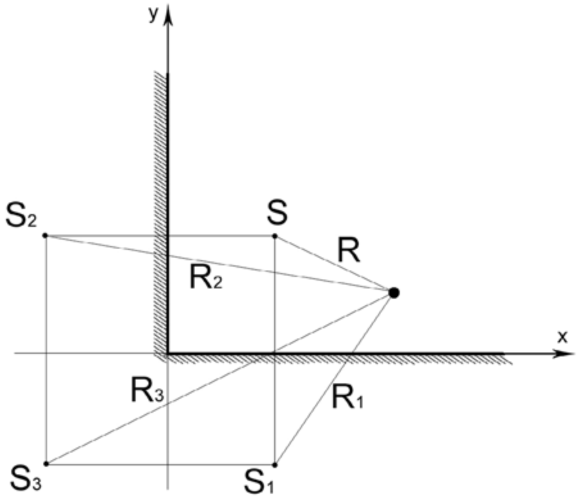

Figure 3. Geometric-optics contribution for line source excitation.

[25] The behavior of the field scattered by the DNG cavity may be examined at large distance by considering

$$E_{1z}^{d}|_{u\to\infty, Im(c)<0} \approx \frac{e^{-jk\rho+j\pi/4}}{\sqrt{k\rho}} P^{(e)}(\phi; u_0, v_0), \tag{44}$$

where

$$P^{(e)}(\phi; u_0, v_0) = 16 \sum_{l=1}^{\infty} \frac{(-1)^l}{N_{2l}^{(o)}} e_l \mathrm{Ro}_{2l}^{(4)}(c, u_0) \times \mathrm{So}_{2l}(c, v)\mathrm{So}_{2l}(c, v_0) \tag{45}$$

is a far-field coefficient that depends not only on the angle of observation ϕ but also on the source location (u_0, v_0). In the derivation of (45), $\mathrm{Ro}_{2l}^{(4)}(c, u)$ in (39) was evaluated with an asymptotic expansion for the Mathieu radial function.

4.2. H Polarization

[26] The derivations are similar to those for E polarization, hence only the results are given. For a magnetic line source parallel to the z axis and located outside the trench at $(x_0, y_0) \equiv (u_0, v_0) \equiv (\xi_0, \eta_0)$ the primary magnetic field is

$$\boldsymbol{H}^i = \hat{z}H_z^i = \hat{z}H_0^{(2)}(kR). \tag{46}$$

Once again, the total magnetic field in medium 1, H_{1z}, may be written as the sum of diffracted field and the geometrical-optics field. The geometrical-optics field H_{1z}^{go} is the total field that would be present in the absence of the trench and is the sum of the fields due to four line sources, i.e., the primary line source and its three images

$$H_{1z}^{go} = H_0^{(2)}(kR) + H_0^{(2)}(kR_1) + H_0^{(2)}(kR_2) + H_0^{(2)}(kR_3), \tag{47}$$

$$H_{1z}^{go} = 16 \sum_{l=0}^{\infty} \frac{l}{N_{2l}^{(e)}} \mathrm{Re}_{2l}^{(1)}(c, u_<)\mathrm{Re}_{2l}^{(4)}(c, u_>) \times \mathrm{Se}_{2l}(c, v)\mathrm{Se}_{2l}(c, v_0). \tag{48}$$

[27] The diffracted field H_{1z}^{d} due to the presence of the trench in ($x \geq 0$, $y \geq 0$) and the total field inside the trench are given by

$$H_{1z}^{d} = 16 \sum_{l=0}^{\infty} \frac{g_l}{N_{2l}^{(e)}} \mathrm{Re}_{2l}^{(4)}(c, u_0)\mathrm{Re}_{2l}^{(4)}(c, u) \times \mathrm{Se}_{2l}(c, v)\mathrm{Se}_{2l}(c, v_0), \tag{49}$$

$$\begin{aligned} H_{2z} = 16 \sum_{l=0}^{\infty} \frac{h_l}{N_{2l}^{(e)}} &\mathrm{Re}_{2l}^{(4)}(-c, u_0) \\ &\times \left[\frac{\mathrm{Re}_{2l}^{(4)\prime}(-c, u_1)}{\mathrm{Re}_{2l}^{(1)\prime}(-c, u_1)} \mathrm{Re}_{2l}^{(1)}(-c, u) - \mathrm{Re}_{2l}^{(4)}(-c, u) \right] \\ &\times \mathrm{Se}_{2l}(-c, v)\mathrm{Se}_{2l}(-c, v_0). \end{aligned} \tag{50}$$

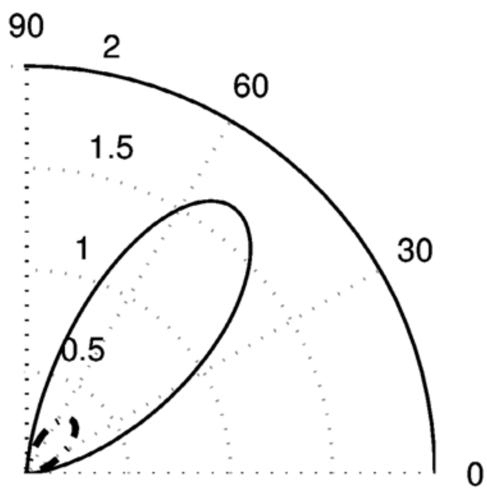

Figure 4. Polar plot of the normalized bistatic RCS $\sigma^{(e)}(\phi)$ given by equation (18) on a linear scale for an E-polarized plane wave incident at an angle $\phi_0 = \pi/4$. Dash-dotted line, $c = 2$; and solid line, $c = 3$. The values for $c = 1$ are so much smaller that they correspond to the origin in the scale used for this plot.

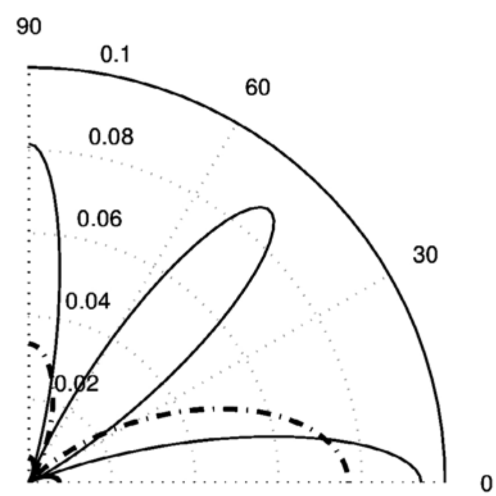

Figure 5. Polar plot of the normalized bistatic RCS $\sigma^{(h)}(\phi)$ given by equation (30) on a linear scale for an H-polarized plane wave incident at an angle $\phi_0 = \pi/4$. Thick solid line, $c = 1$; dash-dotted line, $c = 2$, and thin solid line, $c = 3$.

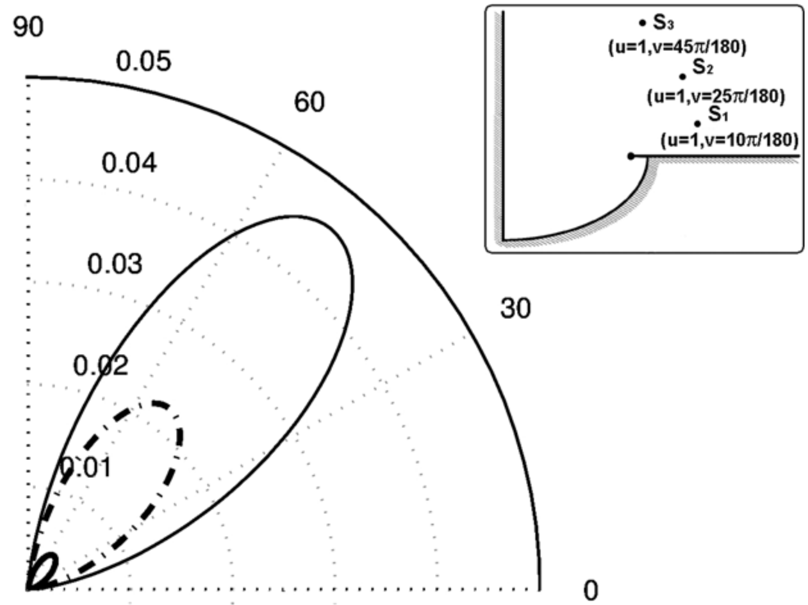

Figure 6. Polar plot of the far-field coefficient $\psi^{(e)}(\phi; u_0, v_0)$ given by equation (57) using a linear scale. The results represent a line source at S_1 (thick solid line); S_2 (dash-dotted line); and S_3 (thin solid line). In all three cases $c = 2$. Units are $(\mathrm{V/m})^2$.

[28] The electric field is related to the magnetic field by (25). The unknown modal coefficients g_l and h_l are determined by applying the boundary condition across $u = 0$, yielding

$$g_l = \mathrm{Re}_{2l}^{(1)}(c,0)\mathrm{Re}_{2l}^{(4)}(c,u_0)\mathrm{Re}_{2l}^{(4)}(-c,u_0) \times \frac{\mathrm{Re}_{2l}^{(4)\prime}(-c,0)}{\Delta_4}, \quad (51)$$

$$h_l = \frac{\mathrm{Re}_{2l}^{(4)\prime}(c,0)\mathrm{Re}_{2l}^{(4)}(c,u_0)\mathrm{Re}_{2l}^{(1)}(c,0)\mathrm{Re}_{2l}^{(4)}(c,u_0)}{\Delta_4}, \quad (52)$$

where

$$\Delta_4 = \mathrm{Re}_{2l}^{(4)}(c,u_0)\mathrm{Re}_{2l}^{(4)}(-c,u_0)\Big[\mathrm{Re}_{2l}^{(4)\prime}(c,0) \times \left(\frac{\mathrm{Re}_{2l}^{(4)\prime}(-c,u_1)}{\mathrm{Re}_{2l}^{(1)\prime}(-c,u_1)}\mathrm{Re}_{2l}^{(1)}(-c,0) - \mathrm{Re}_{2l}^{(4)}(-c,0)\right) - \mathrm{Re}_{2l}^{(4)}(c,0)\mathrm{Re}_{2l}^{(4)\prime}(-c,0)\Big]. \quad (53)$$

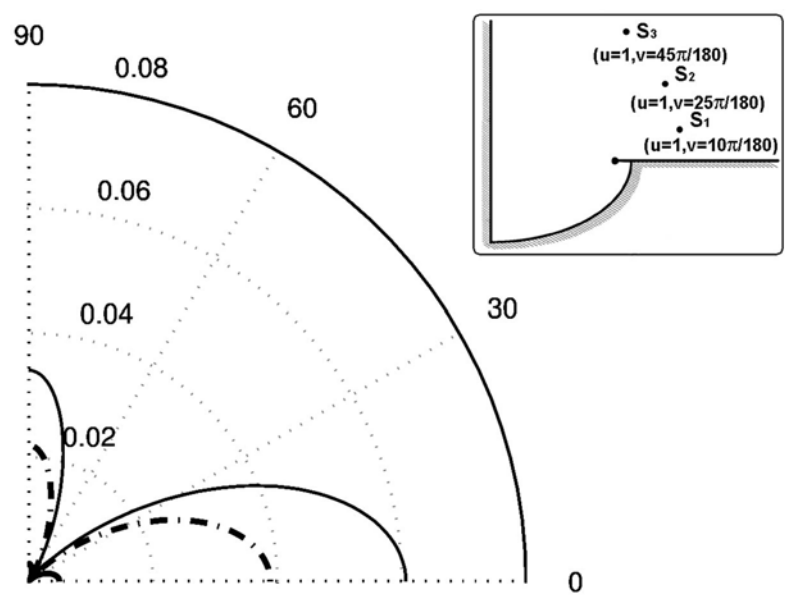

Figure 7. Polar plot of the far-field coefficient $\psi^{(h)}(\phi; u_0, v_0)$ given by equation (58) using a linear scale. The results represent a line source at S_1 (thin solid line); S_2 (dash-dotted line); and S_3 (thick dash line). In all three cases $c = 2$. Units are $(\mathrm{V/m})^2$.

Table 1. Normalized Bistatic RCS

ϕ_0	$c = 1$	$c = 2$	$c = 3$
10°	1.83634E-05	3.18010E-02	2.49653E-01
20°	6.57825E-05	1.19100E-01	1.01212E+00
30°	1.22011E-04	2.36298E-01	2.25958E+00
40°	1.61991E-04	3.40340E-01	3.74171E+00
50°	1.66586E-04	3.81127E-01	4.83292E+00
60°	1.32244E-04	3.27360E-01	4.72363E+00
70°	7.44216E-05	1.96273E-01	3.13648E+00
80°	2.13644E-05	5.86993E-02	1.00117E+00

[29] Similarly, the behavior of the field scattered magnetic field by the DNG cavity may be examined at large distance by considering

$$H^d_{1z}|_{u\to\infty, Im(c)<0} \approx \frac{e^{-jk\rho+j\pi/4}}{\sqrt{k\rho}} P^{(h)}(\phi; u_0, v_0), \quad (54)$$

where

$$P^{(h)}(\phi; u_0, v_0) = 16\sum_{l=1}^{\infty} \frac{(-1)^l}{N^{(e)}_{2l}} g_l \mathrm{Re}^{(4)}_{2l}(c, u_0) \times \mathrm{Se}_{2l}(c, v)\mathrm{Se}_{2l}(c, v_0) \quad (55)$$

is a far-field coefficients that depends not only on the angle of observation ϕ but also on the source location (u_0, v_0).

5. Numerical Results

[30] The evaluation of Mathieu functions was accomplished using the Fortran code described by *Erricolo* [2006]. The numerical results described in this section were obtained after summing the first 20 terms of the pertinent series and using the acceleration method described by *Erricolo* [2003].

5.1. Plane Wave Incidence

[31] The scattering effect of trench can be investigated easily by looking at the normalized bistatic RCS as given by (18) and (30). The value of c is controlled by the frequency and the focal distance d through

$$c = \frac{kd}{2} = \frac{\pi d}{\lambda}. \quad (56)$$

[32] What is important is the relative value of parameters inside and outside the trench, not their absolute value. Since the medium outside the trench is of infinite extent, it may be safely assumed to be free space; however, this restriction is not necessary for the validity of our calculations.

[33] The effect of the variation of c is examined in Figure 4, where an E-polarized plane wave is incident at an angle $\varphi_0 = \pi/4$. Three cases were examined: $c = 1$, $c = 2$, and $c = 3$. When $c = 1$ the RCS is so much smaller than for the other two cases that it simply appears as a point at the origin of the polar diagram. The observed behavior of higher RCS values when c is increased agrees with what is expected from scattering theory.

[34] Figure 5 shows the effect of the variable c values with an H-polarized plane wave with same incident angle.

5.2. Line Source Incidence

[35] The scattering effect of trench can be easily investigated by looking at the square magnitude of the far-field coefficient (45)

$$\psi^{(e)}(\phi; u_0, v_0) = \left|P^{(e)}(\phi; u_0, v_0)\right|^2 \quad (57)$$

for an E polarized line source.

[36] Figure 6 shows the far-field behavior for three different locations of the electric line source along the ellipse $u = 1$, for a corner gap with $c = 2$ and $u_1 = 0.5$. Our results indicate that the most noticeable effect of an angular variation in the location of the line source is to change the intensity of the far field pattern. Specifically, the intensity is stronger when the line source is farther from both metallic surfaces as one would expect. The direction of the maximum is scattered around the 50° direction and it varies depending on the specific case.

[37] Similarly, the scattering effect of a magnetic line source may be investigated by looking at the square magnitude of the far-field coefficient (55)

$$\psi^{(h)}(\phi; u_0, v_0) = \left|P^{(h)}(\phi; u_0, v_0)\right|^2 \quad (58)$$

for an H polarized line source, which is shown in Figure 7.

[38] One observes that a variation in the angular location of the line source causes a variation in the intensity of the far field pattern. Contrary to the E polarization case, the intensity is stronger when the line source is closer to the metallic surfaces. For each line source location, there are two far field pattern maxima along the x and y axes, but the one along the x axis is always stronger, as it was observed for other cases that were not plotted in Figure 7.

[39] Table 1 provides some values of the normalized bistatic RCS (18) for different values of c and of the incidence angle φ_0; in all cases, $v = 50\pi/180$ and $u_1 = 0.5$. These values were obtained by summing the first 10 terms of the series and then by comparing them with the sum of the first 20 terms of the series. They are accurate up to the first six significant digits.

6. Conclusion

[40] An exact solution to the boundary value problem of a trench of quarter-elliptical cross section filled with DNG metamaterial, slotted along its interfocal strip and flush mounted in the corner of two metallic walls perpendicular to each other has been obtained by separation of variables in the frequency domain, for both plane wave and line source excitations. Numerical results have been shown for the far-field coefficient.

[41] Our result enriches the catalog of canonical solutions for two-dimensional boundary value problems, and may be useful in validating computer codes that have been developed for complex geometries and penetrable media.

[42] **Acknowledgments.** This work was partially supported under the USA DOD/AFOSR grant FA9550-05-1-0443.

References

Akgol, O., D. Erricolo, and P. Uslenghi (2009a), Electromagnetic scattering by a semielliptical trench filled with DNG metamaterial, in *International Conference on Electromagnetics in Advanced Applications ICEAA*, pp. 1034–1037, Inst. of Electr. and Electr. Eng., New York.

Akgol, O., D. Erricolo, and P. Uslenghi (2009b), Radiation of a line source by a slotted semielliptical trench filled with DNG metamaterial, in *Symposium on Microwave, Antenna, Propagation and EMC Technologies for Wireless Communications, 2009*, pp. 107–110, Inst. of Electr. and Electr. Eng., New York.

Bowman, J. J., T. B. A. Senior, and P. L. E. Uslenghi (1987), *Electromagnetic and Acoustic Scattering by Simple Shapes*, Hemisphere Publishing, New York.

Erricolo, D. (2003), Acceleration of the convergence of series containing Mathieu functions using Shanks transformation, *IEEE Antennas Wireless Propag. Lett.*, *2*, 58–61.

Erricolo, D. (2006), Algorithm 861: Fortran 90 subroutines for computing the expansion coefficients of Mathieu functions using Blanch's algorithm, *ACM Trans. Math. Software*, *32*(4), 622–634.

Erricolo, D., and P. L. E. Uslenghi (2005), Penetration, radiation, and scattering for a cavity-backed gap in a corner, *IEEE Trans. Antennas Propag.*, *53*(8), 2738–2748.

Staff of the Computation Laboratory (1967), *Tables Relating to Mathieu Functions*, *Appl. Math. Ser.*, vol. 59, 2nd ed., U.S. Gov. Print. Off., Washington, D. C.

Stratton, J. A. (1941), *Electromagnetic Theory*, McGraw-Hill, New York.

Uslenghi, P. (1992), Exact scattering from a slotted semielliptical channel, in *Proceedings of the IEEE AP-S International Symposium*, pp. 1849–1852, Inst. of Electr. and Electr. Eng., New York.

Uslenghi, P. (1999), Exact electromagnetic penetration through a gap in a corner, in *Proceedings of 1999 IEEE-APS/URSI International Symposium*, p. 164, Inst. of Electr. and Electr. Eng., New York.

Uslenghi, P. (2004a), Exact geometrical optics scattering from a tri-sector isorefractive wedge structure, *IEEE Antennas Wireless Propag. Lett.*, *3*, 94–95.

Uslenghi, P. (2004b), Exact penetration, radiation and scattering for a slotted semielliptical channel filled with isorefractive material, *IEEE Trans. Antennas Propag.*, *52*(6), 1473–1480.

Ziolkowski, R. W., and E. Heyman (2001), Wave propagation in media having negative permittivity and permeability, *Phys. Rev. E*, *64*(5), 056625, doi:10.1103/PhysRevE.64.056625.

O. Akgol, D. Erricolo, and P. L. E. Uslenghi, Department of Electrical and Computer Engineering, University of Illinois at Chicago, 851 South Morgan St., Chicago, IL 60607, USA. (oakgol2@uic.edu; erricolo@ece.uic.edu; uslenghi@uic.edu)